PNAS RESEARCH ARTICLE | CELL BIOLOGY OPEN ACCESS

Combinatorial clustering of distinct DNA motifs directs synergistic binding of *Caenorhabditis elegans* dosage compensation complex to X chromosomes

Nicholas J. Fuda[a,b,1], Katjuša Brejc[a,b,1], William S. Kruesi[a,b,1], Edward J. Ralston[a,b], Rachel Bigley[a,b], Aram Shin[a,b], Miki Okada[a,b], and Barbara J. Meyer[a,b,2]

Contributed by Barbara Meyer; received July 8, 2022; accepted August 8, 2022; reviewed by David Greenstein and James M. Berger

Organisms that count X-chromosome number to determine sex utilize dosage compensation mechanisms to balance X-gene expression between sexes. Typically, a regulatory complex is recruited to X chromosomes of one sex to modulate gene expression. A major challenge is to determine the mechanisms that target regulatory complexes specifically to X. Here, we identify critical X-sequence motifs in *Caenorhabditis elegans* that act synergistically in hermaphrodites to direct X-specific recruitment of the dosage compensation complex (DCC), a condensin complex. We find two DNA motifs that collaborate with a previously defined 12-bp motif called MEX (motif enriched on X) to mediate binding: MEX II, a 26-bp X-enriched motif and Motif C, a 9-bp motif that lacks X enrichment. Inserting both MEX and MEX II into a new location on X creates a DCC binding site equivalent to an endogenous recruitment site, but inserting only MEX or MEX II alone does not. Moreover, mutating MEX, MEX II, or Motif C in endogenous recruitment sites with multiple different motifs dramatically reduces DCC binding in vivo to nearly the same extent as mutating all motifs. Changing the orientation or spacing of motifs also reduces DCC binding. Hence, synergy in DCC binding via combinatorial clustering of motifs triggers DCC assembly specifically on X chromosomes. Using an in vitro DNA binding assay, we refine the features of motifs and flanking sequences that are critical for DCC binding. Our work reveals general principles by which regulatory complexes can be recruited across an entire chromosome to control its gene expression.

X-chromosome dosage compensation | condensin | DNA binding motifs | genome editing | *C. elegans*

Significance

Diverse regulatory mechanisms balance X-chromosome gene expression between sexes in mammals, fruit flies, and nematodes (XY/XO males and XX females/hermaphrodites). We identify DNA motifs on X that recruit dosage compensation complexes (DCCs) in nematode hermaphrodites to reduce X-chromosome expression. Recruitment sites on X, but not regions on autosomes, contain diverse combinations of different motifs or multiple copies of one motif. DCC binding studies in vivo and in vitro of wild-type and mutant X-recruitment sites validate motif usage. We find that clustering of motifs in different combinations with appropriate orientation and spacing promotes synergy in DCC binding, thereby triggering DCC assembly specifically along X. We demonstrate how regulatory complexes can be recruited across an entire chromosome to control its gene expression.

Anomalies in chromosome dose have the potential to disrupt the balance of gene expression and thereby decrease organismal fitness and viability (1, 2). Unlike imbalances in chromosome dose that cause pathologies, differences in X-chromosome dose that determine sex are well tolerated in diverse species. Dosage compensation mechanisms evolved to balance X-chromosome gene expression between the sexes (XY or XO males and XX females or hermaphrodites), permitting them to tolerate differences in X dose. Dosage compensation strategies differ, but typically a regulatory complex is targeted to X chromosomes of one sex to modulate gene expression (3–7). Human and mouse XX females randomly inactivate one X chromosome (3, 8), *Drosophila melanogaster* XY males increase transcription from their single X chromosome (6, 9), and *Caenorhabditis elegans* XX hermaphrodites reduce transcription from both X chromosomes to balance X-gene expression between sexes (4, 5, 10). For all species, a major challenge has been to define the special features of X chromosomes that recruit the different dosage compensation complexes specifically to X chromosomes (4, 5, 7, 8, 11). Here we define essential X-chromosome sequence features for *C. elegans*.

To achieve balanced X-chromosome gene expression between sexes, *C. elegans* utilizes a dosage compensation complex (DCC) that shares subunits with condensin, a protein complex that controls the organization, resolution, and segregation of mitotic and meiotic chromosomes from yeast to man (4, 5, 12–16). DCC condensin subunits remodel the topology of X chromosomes during dosage compensation (17, 18). They are targeted to X chromosomes of XX hermaphrodites by proteins that coordinately control both sex determination and dosage compensation (SDC-2 and SDC-3) in response to the X signal that specifies sex (19–21). SDC-2, a 350-kDa protein with no known homologs outside nematodes, is the sole dosage compensation protein expressed exclusively in hermaphrodites and thereby controls both the sex specificity and X specificity of dosage compensation (19). Although all DCC subunits require SDC-2 for their binding to X in vivo, SDC-2 can bind to X by itself. SDC-3, a zinc-finger protein, assists SDC-2 in the X-recruitment process (20) as does DPY-30 (22).

Author contributions: N.J.F., K.B., W.S.K., E.J.R., and B.J.M. designed research; N.J.F., K.B., W.S.K., E.J.R., R.B., A.S., and M.O. performed research; N.J.F., K.B., W.S.K., E.J.R., R.B., A.S., M.O., and B.J.M. analyzed data; and N.J.F., K.B., and B.J.M. wrote the paper.

Reviewers: D.G., University of Minnesota Twin Cities; and J.M.B., Johns Hopkins Medical Institute.

The authors declare no competing interest.

[1]N.J.F., K.B., and W.S.K. contributed equally to this work.

[2]To whom correspondence may be addressed. Email: bjmeyer@berkeley.edu.

This article contains supporting information online at http://www.pnas.org/lookup/suppl/doi:10.1073/pnas.2211642119/-/DCSupplemental.

Published September 6, 2022.

Maximal reduction of X-chromosome gene expression in hermaphrodites by the DCC is only achieved once the histone modification H4K20me1 is enriched on X. The DCC subunit called DPY-21 accomplishes that task. DPY-21 is a Jumonji C histone demethylase that converts H4K20me2 to H4K20me1 (23). H4K20me1 enrichment modulates the three-dimensional structure of X chromosomes (23).

Directed by SDC-2, the DCC binds in a sequence-dependent manner to its major *cis*-acting sites on X called recruitment elements on X (*rex*) sites (24, 25). Once bound to X, the DCC spreads along the entire chromosome in a sequence-independent manner to sites, typically found in gene promoters, which exhibit lower DCC occupancy than at *rex* sites (18, 22, 25–27). Maximal DCC occupancy at these secondary sites requires their association with *rex* sites in *cis*. SUMOylation of recruitment protein SDC-3 and some condensin subunits is required for the sex-specific assembly and function of the DCC on X (28). Stable DCC binding near a gene is neither necessary nor sufficient for the dosage compensation of that gene, indicating the DCC can act at a distance (29).

Initially, *rex* sites were defined by their ability to recruit the DCC when detached from X and present in multiple copies on extrachromosomal arrays in embryos or adult gut cells (24, 27). Additional *rex* sites were identified by chromatin immunoprecipitation (ChIP) experiments using DCC antibodies and verified by functional analysis of DCC binding in vivo to captured DNA using extrachromosomal array assays (25). Sequence analysis of multiple *rex* sites revealed a 12-bp motif named motif enriched on X (MEX) (Fig. 1*A*) (25). MEX motifs with varying degree of match to the consensus sequence are enriched between 4- and 25-fold on X chromosomes (Fig. 1 *B* and *C*), and mutational analysis revealed they are required for autonomous DCC recruitment to a subset of *rex* sites (18, 25, 26). However, only 55% of the analyzed *rex* sites have a high-scoring MEX motif coincident with high DCC occupancy (*SI Appendix*, Table S1). These results revealed the importance of MEX in recruiting the DCC to X but also indicated that MEX cannot be the sole determinant of X specificity or DCC assembly on X.

Our genomics approaches used here identify additional DNA motifs that recruit the DCC, and we demonstrate their importance in DCC recruitment by systematic analysis of DCC binding in vivo and in vitro to wild-type *rex* sites and mutant *rex* derivatives carrying altered motifs. Moreover, our results show that clustering of motifs in different combinations within *rex* sites promotes synergy in DCC binding and thereby triggers DCC assembly specifically on X chromosomes.

Results

Identification of Motifs on X That Recruit the DCC. To identify additional motifs that recruit the DCC to X chromosomes, seven strong SDC-3 ChIP-seq peaks that lacked MEX motifs were searched for motifs using the program wconsensus (30). These searches identified a motif that was enriched on X chromosomes, and further optimization of the motif using 12 strong SDC-3 peaks resulted in the 26-bp MEX II motif (motif enriched on X II) (Fig. 1*D*). Several features of MEX II made it a strong candidate to participate in DCC recruitment. First, MEX II is enriched up to 50-fold on X chromosomes (Fig. 1*E*). Second, strong matches to the MEX II consensus sequence reside in 13 of 48 *rex* sites (*SI Appendix*, Table S1), and the peak of SDC-3 binding at these sites overlaps the motifs (Fig. 1*F*). No SDC-3 binding occurs at the 22 MEX II motifs on autosomes, all of which have a weaker consensus match (ln[P] value < −16.0) (Fig. 1*F* and *SI Appendix*, Table S2). In the genome, of the 13 MEX II motifs with a score of −18.18 or less, 12 are on X chromosomes and 10 are in the identified *rex* sites (*SI Appendix*, Tables S1 and S2). Third, high-scoring MEX II motifs can recruit the DCC condensin subunit DPY-27 when detached from X and present in multiple copies on extrachromosomal arrays made from a 2-kb region that has a high-scoring MEX II motif from X and strong endogenous SDC-3 and DPY-27 ChIP-seq signals (*rex-43*) (Fig. 1 *J* and *K*). In contrast, extrachromosomal arrays made from a 2-kb region that had modest SDC-3 ChIP-seq signal but lacked any motif (*dox-50*) failed to recruit DPY-27 (Fig. 1*J*). These results implicate MEX II as a critical element for DCC recruitment to X.

To assess whether additional motifs might participate in DCC recruitment, the MEME program (31) was used to search for motifs in sequences from the 25 strongest SDC-3 peaks in which the 5′ MEX II sequence TGTGGATAA was converted to Ns, as were all MEX motifs stronger than ln(P) < −13. The most significantly enriched motif, termed Motif C, is a 9-bp sequence (Fig. 1*G*). Although Motif C is not preferentially enriched on X (Fig. 1*H*), sequences with strong matches to Motif C are present in centers of large DCC peaks (Fig. 1*I*), similar to MEX and MEX II motifs. Motif C variants are found in 11 of 12 *rex* sites on X that lack strong MEX and MEX II motifs and are also present in *rex* sites with MEX and MEX II motifs (*SI Appendix*, Table S1). A 2-kb region that included such variants (GGGCAGGGG, GCGAAGGGG, and GCTAAGGGG) recruited the DCC when detached from X, suggesting their importance in DCC binding and in predicting *rex* sites on X (*rex-46*, Fig. 1*J*).

Synergistic Binding to Clustered DNA Motifs In Vivo Triggers DCC Assembly on X. The importance of MEX II in recruiting the DCC to X chromosomes was revealed by inserting MEX II and MEX motifs in different combinations and orientations into an ectopic location on X using genome editing and then performing ChIP qPCR to assess SDC-3 binding (Fig. 2 *A* and *B* and *SI Appendix*, Fig. S1*A*). Six different combinations of MEX II (ln[P] score of −21.84) and MEX (ln[P] score of −17.52) from *rex-32* were created and inserted into X at location 3,151,210 bp, a site lacking SDC-3 binding within 100 kb. The insertions included: 1) wild-type MEX II and MEX with 13-bp separation as in *rex-32*; 2) mutant MEX II and mutant MEX; 3) mutant MEX II and wild-type MEX; 4) wild-type MEX II and mutant MEX; 5) wild-type MEX II and MEX with a 5-bp separation; and 6) wild-type MEX II and wild-type reverse complement of MEX (Fig. 2*B* and *SI Appendix*, Fig. S1*A*).

SDC-3 binding was absent from the endogenous unedited site in wild-type embryos, but it increased to the level of binding at *rex-46* when both MEX II and MEX motifs were inserted (Fig. 2 *A* and *B*). Binding was lower than that at *rex-1* or *rex-43* (Fig. 2*A*). SDC-3 binding to the insertion site required both motifs, since mutating either MEX II or MEX strongly decreased binding (Fig. 2*B*). The sum of SDC-3 binding at the sites with either MEX II or MEX alone was lower than the level of SDC-3 binding at a site with both motifs, indicating that DCC binding was synergistic. Reducing the spacing between motifs to 5 bp or flipping the orientation of the MEX motif decreased SDC-3 binding, indicating that SDC-3 binding requires proper distance between motifs and proper relative orientation (Fig. 2*B*).

Synergy in DCC binding to MEX II and MEX motifs was demonstrated further by mutational analysis of the endogenous *rex-1* site using genome editing (Fig. 2*C* and *SI Appendix*, Fig. S1*B*).

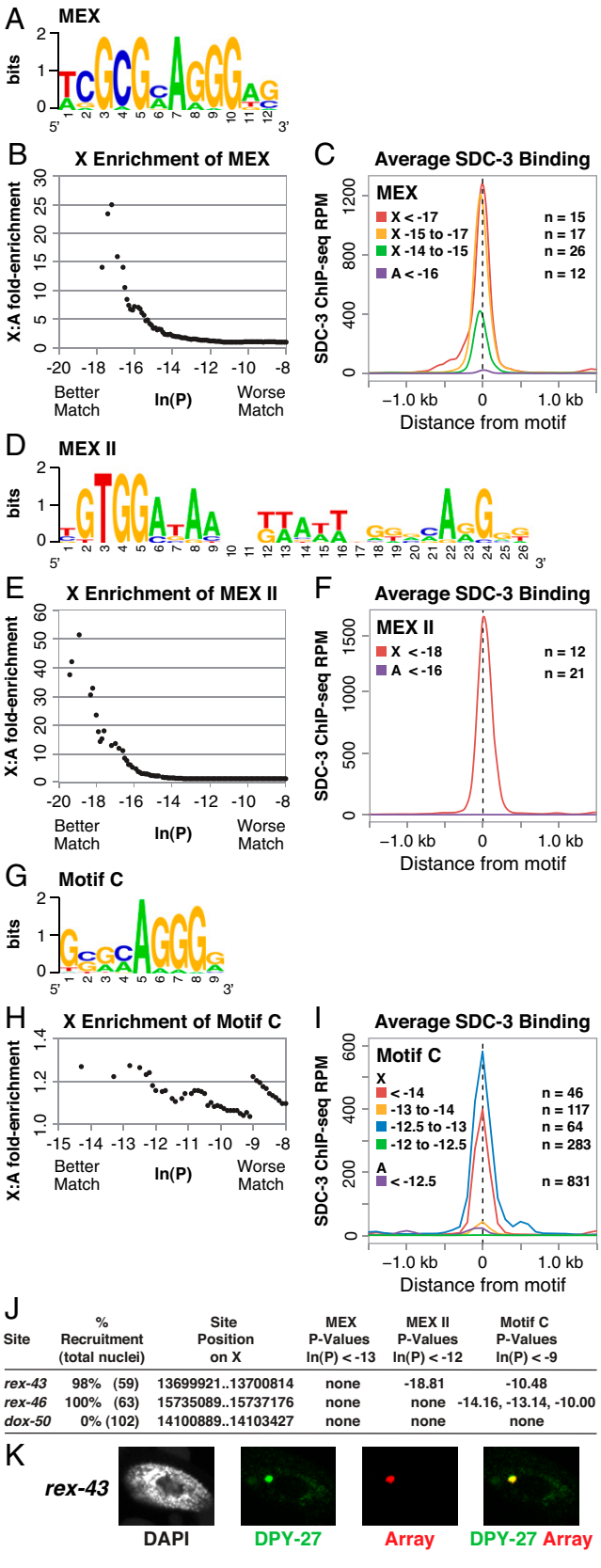

Site	% Recruitment (total nuclei)	Site Position on X	MEX P-Values ln(P) < -13	MEX II P-Values ln(P) < -12	Motif C P-Values ln(P) < -9
rex-43	98% (59)	13699921..13700814	none	-18.81	-10.48
rex-46	100% (63)	15735089..15737176	none	none	-14.16, -13.14, -10.00
dox-50	0% (102)	14100889..14103427	none	none	none

Fig. 1. DNA motifs on X that recruit the dosage compensation complex. (*A*) Consensus motif for the 12-bp MEX motif. (*B*) The MEX motif is enriched up to 25-fold on X chromosomes relative to autosomes. Plot shows the fold enrichment (*y* axis) of MEX variants (*x* axis) on X compared to autosomes. ln(P) is the natural log of the probability that the 12-mer matches the MEX consensus motif matrix as calculated by the Patser program. The lower the score, the better the match. The maximum ln(P) value for MEX is −18.85. (*C*) Bound DCC levels are highest on the highest scoring MEX motifs. Graph shows average SDC-3 ChIP-seq signal (reads per million mapped reads) across a 3-kb window surrounding the high-scoring MEX motifs for three groups on X: (ln[P] < −17, −17 to −15, −15 to −14) and autosomes (ln[P] < −16). n indicates the number of motifs averaged for each group. (*D*) Consensus motif for the 26-bp MEX II motif. (*E*) The MEX II motif is enriched up to 50-fold on X chromosomes relative to autosomes. Plot shows the fold enrichment (*y* axis) of MEX II variants (*x* axis) on X compared to autosomes. The maximum ln(P) value for MEX II is −24.79. (*F*) The DCC is bound to high-scoring MEX II motifs on X but not MEX II motifs on autosomes. Graph shows average SDC-3 ChIP-seq signal (reads per million mapped reads) across a 3-kb window surrounding high-scoring MEX II motifs on X (ln[P] < −18) and on autosomes (ln[P] < −16). n indicates the number of motifs averaged for each group. (*G*) Consensus motif for the 9-bp Motif C. (*H*) Motif C is not enriched on X chromosomes relative to autosomes. Plot shows the fold enrichment (*y* axis) of Motif C variants (*x* axis) on X compared with autosomes. The maximum ln(P) value for Motif C is −14.16. (*I*) Bound DCC levels are highest on the highest scoring Motif C motifs. Average SDC-3 ChIP-seq signal (reads per million mapped reads) across a 3-kb window surrounding the high-scoring Motif C variants for four groups on X (ln[P] < −14, −14 to −13, −13 to −12.5, −12.5 to −12) and on autosomes (ln[P] < −12.5). n indicates the number of motifs averaged for each group. (*J*) *rex* DNA with either MEX II or Motif C sequences recruits the DCC when detached from X chromosomes and present in multiple copies on extrachromosomal arrays. The table shows the percent of nuclei exhibiting DCC recruitment to extrachromosomal arrays containing DNA from the indicated genomic regions for the *rex-43*, *rex-46*, and *dox-50* (dependent on X) sites. ln(P) is the natural log of the *P* value for each motif within the region. (*K*) Image of DCC recruitment to *rex-43* DNA in an extrachromosomal array. Confocal images show an intestinal cell nucleus carrying an extrachromosomal array containing multiple copies of *rex-43* (red, labeled with a FISH probe), costained with DAPI (gray), and antibodies to DPY-27 (green).

Deleting both motifs eliminated SDC-3 binding, and deleting or mutating either motif individually reduced SDC-3 binding dramatically. Adding a MEX motif to wild-type *rex-1* enhanced DCC binding when inserted 5 bp from the endogenous MEX (Fig. 2*C*).

Synergy in DCC binding was also evident for the two MEX II motifs in the endogenous *rex-39* site (Fig. 2*D*). Mutating both motifs eliminated DCC binding, and mutating either motif individually or separating them by 37 bp instead of the wild-type 17 bp caused a reduction in binding (Fig. 2*D* and *SI Appendix*, Fig. S1*C*). Together these results demonstrate the importance of MEX II for recruiting the DCC to X and demonstrate synergy in DCC binding conferred by two motifs, either MEX II motifs or MEX II and MEX motifs.

Clustering of Motif C is also critical for DCC recruitment to *rex* sites. Mutating different combinations of Motif C in the endogenous *rex-46* site using genome editing revealed the synergy in DCC binding to multiple motifs (Fig. 2*E* and *SI Appendix*, Fig. S1*D*). Mutating all three motifs, only the middle motif, only the two flanking motifs, or only the middle motif and a flanking motif resulted in the same dramatic reduction in DCC binding to *rex-46* (Fig. 2*E*). These results imply that DCC occupancy at *rex* sites in vivo can also be enhanced through synergistic DCC interactions mediated by clustered DNA motifs that are not enriched on X chromosomes.

DCC Binding Assay In Vitro. We explored further the features and functions of X motifs that facilitate DCC recruitment by implementing an in vitro assay (*SI Appendix*, Fig. S2 *A* and *B*). This assay utilized embryo extracts made from a nematode strain encoding a 3×FLAG-tagged SDC-2 protein expressed from an extrachromosomal array. The monoclonal FLAG antibody resulted in a better signal-to-noise ratio for our in vitro experiments than antibodies to SDC-3 or DCC condensin subunit DPY-27. Wild-type or mutant 651-bp DNA fragments with biotinylated 5′ ends were coupled to streptavidin-coated magnetic beads and incubated with embryo extracts. The bound

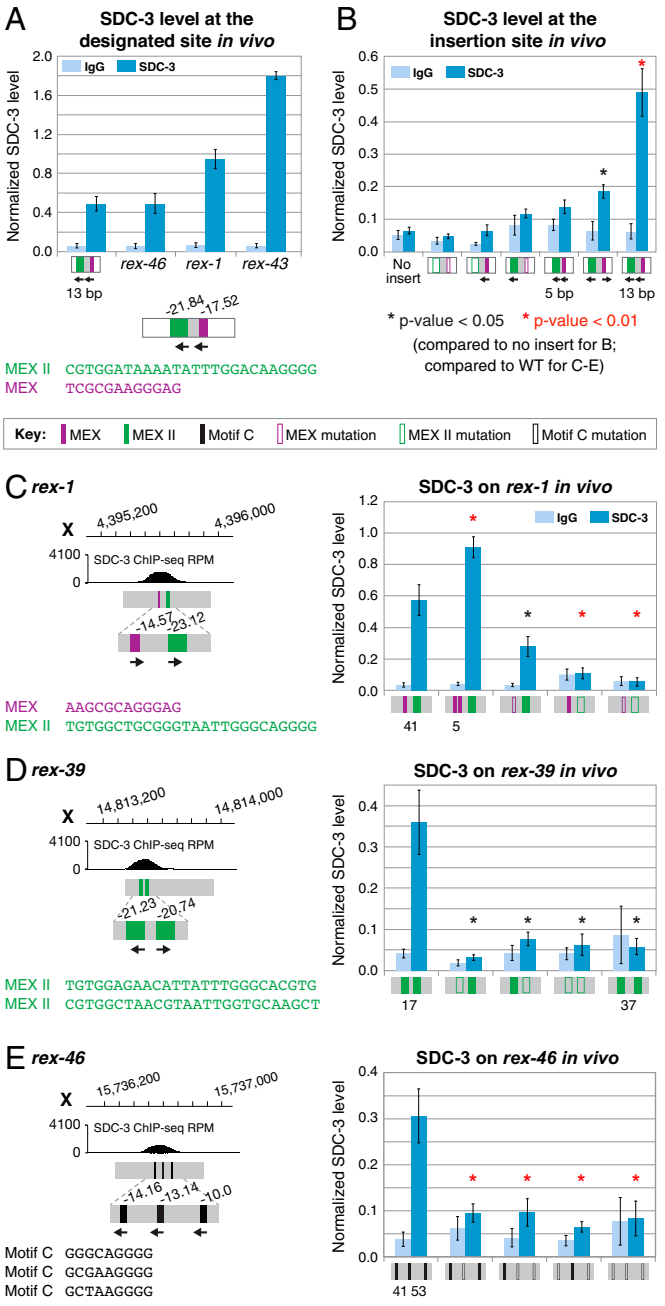

Fig. 2. Synergistic DCC binding to clustered X motifs in vivo. (*A*) Insertion on X of a DNA fragment from *rex-32* containing only MEX and MEX II motifs confers DCC binding at a level comparable to that of endogenous *rex* sites. The schematic below the graph shows the 51-bp *rex-32* fragment spanning MEX II (green) (ln[P] = −21.84), the intervening 13-bp spacer (gray), and MEX (purple) (ln[P] = −17.52) that was inserted at X-chromosome location 3,151,220 bp. The graph shows ChIP qPCR levels of DCC subunit SDC-3 (dark blue) and IgG control (light blue) at the edited site and three endogenous *rex* sites. SDC-3 levels for each replicate were normalized to the average SDC-3 level of all regions assayed, and error bars represent the SEM of four replicates. In *A* and also *B*–*E*, leftward-facing arrows in the schematics indicate the motifs are on X in the reverse complement orientation. Numbers above the motifs are the natural log of the probability (lnP) that the sequence matches the consensus. (*B*) Motif number, spacing, and orientation affect DCC binding in vivo. The graph shows normalized SDC-3 ChIP qPCR (dark blue) levels and control IgG ChIP qPCR (light blue) levels at the wild-type nonedited X site without an insertion, at the site with an insertion having both motifs mutated, just MEX II mutated, just MEX mutated, wild-type MEX II and wild-type MEX separated by a 5-bp spacer instead of the wild-type 13-bp spacer in *rex-32*, wild-type MEX II with MEX in the reverse orientation (rightward arrow) from wild type, as well as wild-type MEX II and MEX with the 13-bp spacer from wild-type *rex-32* in *A*. DNA sequences for wild-type and mutant motifs are in *SI Appendix*, Fig. S1*A*. SDC-3 levels for each replicate were normalized as in *A*, and error bars represent the SEM of four replicates. Asterisks indicate SDC-3 levels significantly higher than the level at the X site with no insertion, as evaluated by the Student's *t* test. (*C*) MEX and MEX II motifs are critical for DCC binding at the endogenous *rex-1* site in vivo. *Left* shows the X-chromosome coordinates, SDC-3 ChIP-seq profile for *rex-1*, a schematic of the MEX (purple) and MEX II (green) motifs within *rex-1*, and the motif ln(P) scores (MEX, −14.57 and MEX II, −23.12), motif orientations, and motif sequences. The *Right* graph shows ChIP qPCR levels for SDC-3 (dark blue) and control IgG (light blue) at endogenous *rex-1* and for mutant sites created using genome editing. Assayed sites include the nonedited site with its 41-bp spacer between MEX and MEX II, as well as mutant sites with the following changes: an extra MEX motif with a 5-bp spacer, a MEX deletion, a MEX II mutation, and a deletion of MEX, the spacer, and MEX II. DNA sequences are in *SI Appendix*, Fig. S1*B*. SDC-3 levels for each replicate were normalized to the average level at seven endogenous nonedited *rex* sites. Error bars represent the SEM of at least three replicates. Asterisks in *C* and in *D* and *E* indicate SDC-3 levels significantly different from those at the nonedited sites, as evaluated by the Student's *t* test. (*D*) Two MEX II motifs with proper spacing are essential for DCC binding at endogenous *rex-39* in vivo. *Left* shows the same type of information for *rex-39* as was described for the *rex* in *C*. The *Right* graph shows the SDC-3 (dark blue) and IgG control (light blue) ChIP qPCR results for the nonedited endogenous *rex-39* site with its two wild-type MEX II motifs separated by 17 bp and for mutant sites created using genome editing: mutation of the upstream MEX II motif, mutation of the downstream MEX II motif, mutation of both motifs, and insertion of an extra 20 bp between MEX II motifs. DNA sequences are in *SI Appendix*, Fig. S1*C*. SDC-3 levels for each replicate were normalized as in *C*. Error bars, SEM of at least three replicates. (*E*) All three Motif C variants are required for DCC binding at endogenous *rex-46* in vivo. *Left* shows the same type of information for *rex-46* as was described for the *rex* in *C*. The *Right* graph shows the SDC-3 and IgG control ChIP qPCR results for endogenous *rex-46* with its three Motif C variants and different mutant versions created using genome editing: mutation of the middle motif, mutation of the two downstream motifs, mutation of only the upstream and the downstream motif, mutation of all three motifs. DNA sequences are in *SI Appendix*, Fig. S1*D*. SDC-3 levels for each replicate were normalized as in *C*. Error bars, SEM of at least three replicates.

proteins were eluted, spotted onto a nitrocellulose membrane, and probed with a monoclonal mouse anti-FLAG antibody. Antigen–antibody complexes were visualized and quantified by chemiluminescence using an imager. Quantities of embryonic extract and *rex-32* DNA or X control DNA (np1) appropriate for the in vitro DNA binding assays were determined by performing extract titration and DNA titration experiments (*SI Appendix*, Fig. S2 *A* and *B*). DNA concentrations that elicited the highest ratio of DCC binding to *rex-32* DNA compared to X control DNA were selected. The X control DNA fragment (np1) lacks DCC binding in vivo and lacks sequences with matches to the motifs.

Like *rex-32*, which has both MEX and MEX II motifs, *rex* sites with high DCC occupancy in vivo and combinations of only MEX, only MEX II, or both MEX II and Motif C exhibited robust SDC-2 binding in vitro when compared to X control DNA (Fig. 3*A*). The *rex* sites also exhibited robust SDC-3 binding in the in vitro assay (*SI Appendix*, Fig. S3*A*), consistent with the roles of both SDC-3 and SDC-2 in recruiting all DCC subunits to X and the colocalization of SDC-2 and SDC-3 at *rex* sites in vivo (22).

Mutational Analysis of DCC Binding to MEX and MEX II In Vitro and In Vivo. Using the in vitro assay, we explored DCC binding to individual motifs and different motif combinations inserted into X control DNA from a region that lacked DCC binding in vivo (np1). A single MEX motif from *rex-32* (TCGCGAAGGGAG) with a strong match to the consensus sequence recruited the DCC in vitro when it was inserted into either of two different X control DNA fragments (Fig. 3*B* and *SI Appendix*, Fig. S3*B*). Moreover, a single MEX II motif from *rex-32* (CGTGGATAAAATATTT GGACAAGGGG) also recruited the DCC robustly (Fig. 3*B* and *SI Appendix*, Fig. S3*B*). Combining the two motifs enhanced

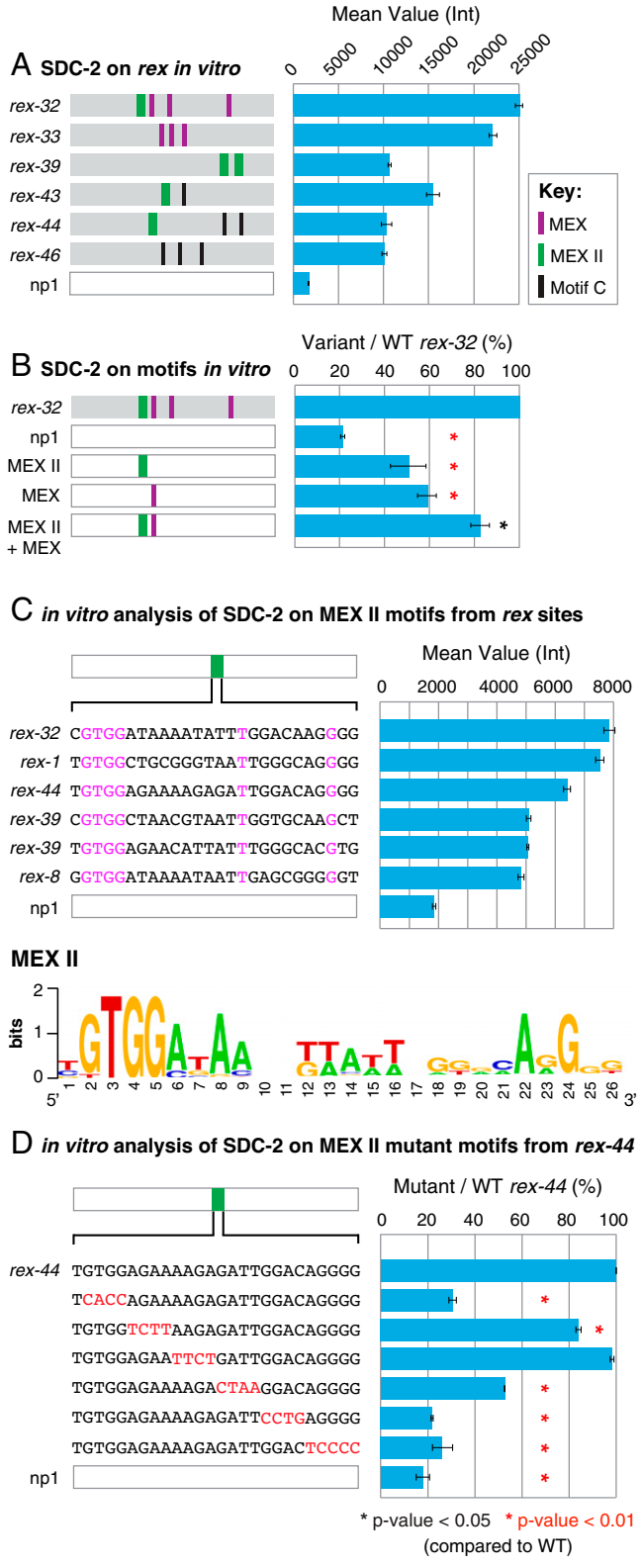

Fig. 3. In vitro assay characterizing binding of SDC-2 to *rex* sites and X motif sequences. (*A*) The presence of multiple binding motifs clustered within a *rex* site results in strong SDC-2 binding in vitro. Each *rex* site contains a cluster of DNA motifs as indicated in the diagrams and key. The X control DNA fragment denoted np1 contains no known DNA motifs and shows no DCC binding in vivo. The plot represents the average of three technical replicates with error bars indicating the SD. (*B*) Individual MEX or MEX II motifs show robust SDC-2 binding. The MEX and MEX II motifs from *rex-32* were introduced into the X control fragment np1. The presence of both motifs enhanced SDC-2 binding compared to binding on a single motif. SDC-2 levels detected for the variant fragments are shown as the percentage (%) of SDC-2 binding to the wild-type *rex-32* fragment. The plot represents the average of three independent experiments, with error bars indicating SD. Asterisks denote values that are significantly different from those of the wild-type *rex-32* fragment using the Student's *t* test. (*C*) MEX II motifs with different matches to the consensus sequence show SDC-2 binding. MEX II motifs from different *rex* sites were introduced into the X control fragment np1. The ln(P) values for MEX II motifs are the following: *rex-32*, −21.84; *rex-1*, −23.12; *rex-44*, −24.79; *rex-39*, −20.74; *rex-39*, −21.23; and *rex-8*, −19.49. Sequences of individual MEX II motifs are shown on the *Left*, with identical nucleotides across all motifs being highlighted in purple. The plot on the *Right* shows quantification of SDC-2 binding to individual fragments containing MEX II. The plot represents the average of three technical replicates with error bars indicating SD. Consensus sequence for MEX II is shown below the plot. (*D*) Identification of MEX II regions required for SDC-2 enrichment on DNA fragments. MEX II from *rex-44*, which has the strongest match to the consensus sequence (ln[P] value: −24.79), was introduced into the X control fragment np1. Blocks of four to five bases were scrambled across MEX II. Substitutions of the 5′ region (GTGG) or the 3′ region (GGACAGGGG) reduce SDC-2 binding levels to those comparable to the X control fragment np1. SDC-2 levels detected for the mutant fragments are shown as the percentage (%) of SDC-2 binding to the wild-type MEX II fragment. The plot represents the average of three independent experiments with error bars indicating SD. Asterisks denote values that are significantly different from those of the wild-type MEX II sequence using the Student's *t* test.

DCC binding, but the binding did not appear to be synergistic (Fig. 3*B* and *SI Appendix*, Fig. S3*B*).

Consistent with the ability of a single MEX or MEX II motif to recruit the DCC when inserted into X control DNA, retaining either the MEX or MEX II motif in *rex-1*, while mutating the other motif, also permitted DCC binding in vitro, but at a reduced level (*SI Appendix*, Fig. S3*C*, *c* and *d* vs. *a*). Similarly, retaining one of the two MEX II motifs in *rex-39*, while mutating the other, permitted DCC binding, but at a reduced level (*SI Appendix*, Figs. S1*C* and S3*D*). Adding a MEX motif to *rex-1* enhanced DCC binding in vitro (*SI Appendix*, Fig. S3*C*, *b* vs. *a*), but not to the same extent as it did in vivo (Fig. 2*C*). Moreover, separating the MEX II motifs in *rex-39* by 37 bp instead of the wild-type 17 bp, reduced DCC binding in vitro (*SI Appendix*, Figs. S1*C* and S3*D*), but to a lesser extent than in vivo. The DNA templates assayed in vitro had the same sequence changes as the endogenous *rex-1* and *rex-39* variants assayed in vivo (*SI Appendix*, Fig. S1 *B* and *C*).

The sequence of DNA surrounding the motifs can also affect DCC binding. For example, DCC binding in vitro to a mutant *rex-1* template that had a wild-type MEX sequence and mutant MEX II sequence was greater than DCC binding to the same MEX motif in the context of control DNA (*SI Appendix*, Fig. S3*C*, *d* vs. *g*). Also, substituting different sequences between the MEX and MEX II motifs in *rex-1* while retaining the same spacing reduced DCC binding in vitro (*SI Appendix*, Fig. S3*C*, *e* vs. *a*).

DCC binding at individual MEX II motifs from different *rex* sites is generally correlated with their degree of similarity to the consensus sequence over the range of ln(P) scores from −19.49 to −24.79 (Fig. 3*C*). The contribution of individual sequence elements in MEX II toward DCC binding in vitro was monitored after mutagenesis of a MEX II motif (Fig. 3*D*). Sequence elements in MEX II include the distinctive sequence GTGG at the 5′ end, an A/T-rich region (ATAA–TT) in the middle of the motif, and a preference for CAGGG at the 3′ end of high-scoring MEX II motifs. Mutating sequences in either the 5′ or 3′ end of MEX II from *rex-44* (ln[P] score of −24.79) severely reduced DCC binding in vitro, while mutating only the variable A/T-rich region did not (Fig. 3*D*). These results indicate that highly conserved elements within MEX II contribute to DCC binding and reinforce the importance of the motif.

The contribution of individual nucleotides in MEX toward DCC binding was also analyzed in vitro and in vivo after template mutagenesis. Starting with a single *rex-32* MEX motif in X control DNA (np1), a single base pair substitution was made in each of the 12 bases, and DCC binding was assayed in vitro. Substitutions in all but one of the 12 base pairs of MEX (G12C) reduced DCC binding significantly in vitro (Fig. 4*A*). In general, base pair substitutions that caused greater deviations from the consensus sequence score also caused greater decreases in DCC binding in vitro. The G12C substitution had the least effect on binding and also had a low impact on the consensus match.

Guided by the substituted nucleotides (C4G, G5A, A7G, and G9A) causing the greatest effect on DCC binding in vitro, we used genome editing to introduce the same changes in the endogenous MEX of *rex-1* and assayed their impact on DCC binding in vivo. These changes were made in the context of *rex-1*, for which the MEX II motif was still present to permit DCC binding in vivo and thereby enable detection of a change in binding with the MEX nucleotide substitutions. The mutations reduced DCC binding, and both C4G and A7G reduced binding to the extent of a complete MEX deletion or a MEX mutant variant with only A and T nucleotides (Fig. 4*B*). These results demonstrate the importance of individual nucleotides within MEX for DCC binding in vivo and in vitro. The effect of single substitutions in vivo was somewhat less than in vitro, suggesting that synergy between the MEX and MEX II motifs in *rex-1* obviated some of the negative impact of the mutation.

Motif C and Flanking Sequences Contribute to DCC Binding In Vitro. The in vitro assay demonstrated the importance of different Motif C variants and flanking sequences for DCC recruitment (Fig. 5*A*). DCC binding to wild-type *rex-46* with its three Motif C variants (GGGCAGGGG, GCGAAGGGG, and GCTAAGGG) was robust, but binding to a mutant *rex-46* variant that lacked all three motifs was indistinguishable from DCC binding to X control DNA (Fig. 5*A*). Retaining the 5′-most variant (GGGCAGGG) while mutating the other two variants had little effect on DCC binding, suggesting that this single Motif C was responsible for much of the binding to *rex-46*. Consistent with that interpretation, mutating this 5′ variant and the 3′-most variant reduced DCC binding dramatically, although some binding was retained by the middle motif. Inserting the three individual motifs into X control DNA (np1) with the same spacing as in *rex-46* did not result in DCC binding, indicating that the 5′ Motif C is necessary but not sufficient (Fig. 5*B*). In contrast, inserting the three motifs and the sequences between them into X control DNA did support the same level of DCC binding as at the wild-type *rex-46* site (Fig. 5*B*). Further experiments showed that the sequence element necessary for DCC binding resides between the 5′ motif and the middle motif (Fig. 5*B*). Removing only it reduced binding to nearly the level as at X control DNA, but removing the sequence between the middle motif and the 3′-most motif had little consequence. Hence, not only is Motif C important for DCC binding, its flanking sequence, which lacks any obvious motifs, also contributes to binding (Fig. 5*B*). Thus far, however, we find no features in common among other sequences that flank Motif C variants in *rex* sites.

Contribution of X Motifs and *rex* Sites to X-Chromosome Structure. Not only do X motifs and *rex* sites facilitate DCC binding to X chromosomes and the consequent repression of X-linked genes, they also contribute to the three-dimensional structure of hermaphrodite X chromosomes. By binding to eight of its high-occupancy *rex* sites with multiple motifs, the

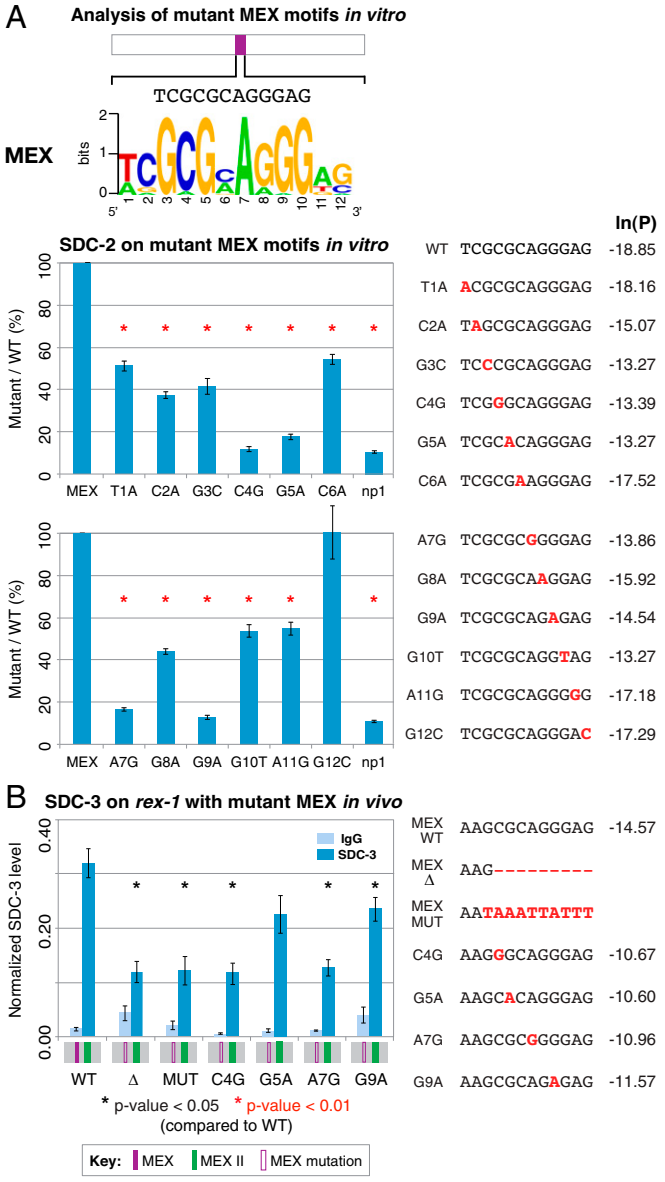

Fig. 4. Single base pair substitutions in the MEX motif reduce DCC binding in vitro and in vivo. (*A*) Quantification of SDC-2 binding in vitro to DNA bearing single base pair substitutions in a MEX motif. A MEX motif with the strongest match to the consensus sequence (ln[P] value of −18.85) was introduced into the X control DNA fragment np1 and was regarded as the wild-type sequence. A single base pair substitution was introduced into each position of the motif, and the DNA was assayed for SDC-2 binding. Substitutions resulted in reduced SDC-2 binding. G12C had the least effect, consistent with its low impact on the consensus match. Substitutions of C4G, G5A, A7G, and G9A completely abolished SDC-2 binding. The SDC-2 levels detected for the mutated fragments are shown as the percentage (%) of SDC-2 binding to the wild-type MEX DNA. The graph represents the average of three independent experiments, with error bars representing SD, and asterisks denote values that are significantly different from those of the wild-type fragment, as evaluated with the Student's *t* test. DNA sequences and ln(P) values of wild-type motifs and those with single base pair substitutions are listed on the *Right*. (*B*) Single base pair substitutions within the MEX motif of *rex-1* can reduce DCC binding in vivo to the same extent as MEX motif removal. *Right* shows the mutant MEX motif variants made in the endogenous *rex-1* MEX motif using genome editing. The plot shows SDC-3 ChIP qPCR levels for nonedited and mutant variants of *rex-1*. The substitutions G5A and G9A reduce SDC-3 binding, and the substitutions C4G and A7G reduce SDC-3 binding to the same extent as a deletion of MEX. SDC-3 levels for each replicate were normalized to the average level at seven different endogenous nonedited *rex* sites. Error bars represent the SEM of at least three replicates. Asterisks indicate SDC-3 levels that are significantly different from the nonedited levels using the Student's *t* test. DNA sequences and ln(P) values of wild-type motifs and those with single base pair substitutions are listed on the *Right*.

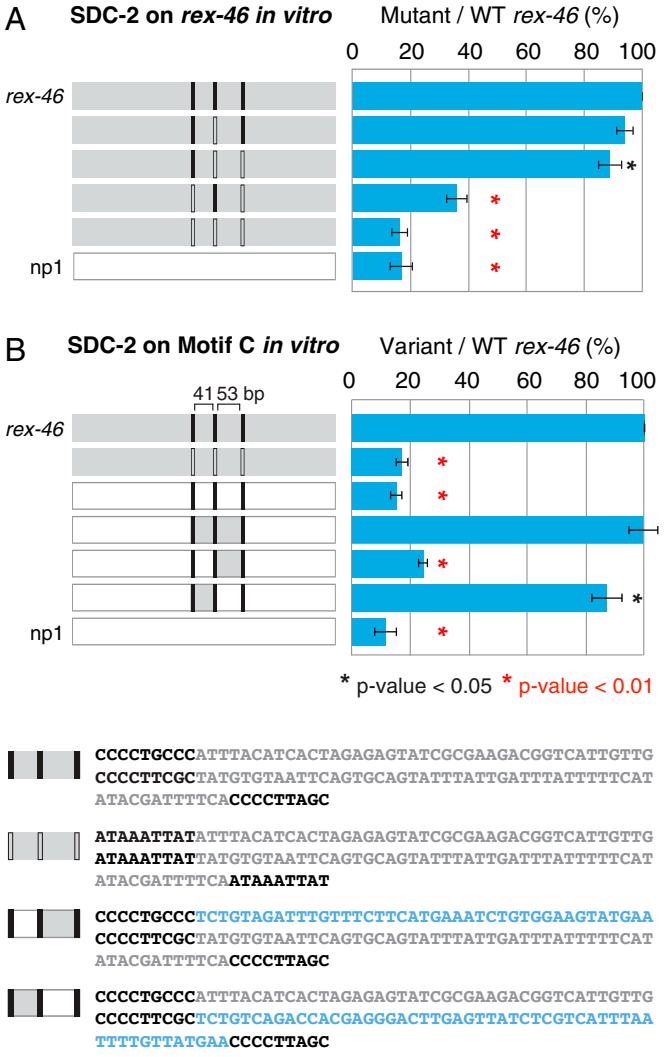

Fig. 5. Motif C and flanking sequences are necessary for SDC-2 recruitment in vitro. (*A*) The wild-type *rex-46* fragment contains three Motif C sequences, and only mutation of all three motifs abolished SDC-2 binding. The levels of SDC-2 binding to the mutant fragments are represented as the percentage (%) of binding to wild-type *rex-46*. The plot represents the average of three independent experiments, with error bars indicating SD. Asterisks denote values that are significantly different from those of wild-type *rex-46* using the Student's *t* test. (*B*) Introducing all three Motif C sequences into the X control fragment np1 is not sufficient for SDC-2 recruitment. Addition of the intervening sequences, particularly between the first and the second Motif C (41-bp fragment) sequences results in SDC-2 binding comparable to that of the wild-type *rex-46* fragment. The SDC-2 levels detected for the variants are shown as percentage (%) of the levels for SDC-2 binding to the wild-type *rex-46* fragment. The plot represents the average of three independent experiments, with error bars indicating SD. Asterisks denote values that are significantly different from those of wild-type *rex-46* using the Student's *t* test. Wild-type and mutant sequences of Motif C elements and the intervening sequences are presented below the graph. The motifs are presented in the reverse complement orientation from the consensus motifs in Fig. 1*G*.

DCC forms boundaries of self-interacting domains (1 Mb) (17, 18) that resemble mammalian topologically associating domains (TADs) (32–34) (Fig. 6 *A* and *B*). Loci in one TAD interact predominantly with each other while being insulated from interactions with loci in neighboring TADs. Perplexing was the observation that motif composition and DCC binding ability were not always predictive of whether a *rex* site formed a TAD boundary (17, 18). Sites such as *rex-32*, which have multiple high-scoring MEX and MEX II motifs and high DCC occupancy formed a strong TAD boundary, but sites such as *rex-23* and *rex-40*, which also have high DCC occupancy in vivo and clustered MEX motifs and Motif C, did not form TAD boundaries (17, 18) (Fig. 6 *A* and *B*). To explore further the features of *rex* sites that contribute to boundary formation, we asked whether high-occupancy *rex* sites that failed to form boundaries at their endogenous locations can form boundaries when inserted into a new location on X that does support *rex*-dependent boundary formation.

First, we inserted *rex-32* into a location in the middle of X that did not have a TAD boundary on the wild-type X and demonstrated that *rex-32* formed a new, strong boundary (Fig. 6*D*). The insertion was in an X chromosome that lacked the eight TAD-forming *rex* sites. Next, we inserted *rex-23* at the same site and found it also supported TAD boundary formation (Fig. 6*E*). Furthermore, inserting *rex-40* also resulted in a TAD boundary (Fig. 6*F*). The strengths of the new boundaries (*rex-32* > *rex-23* > *rex-40*) were correlated with motif composition in the *rex* sites,

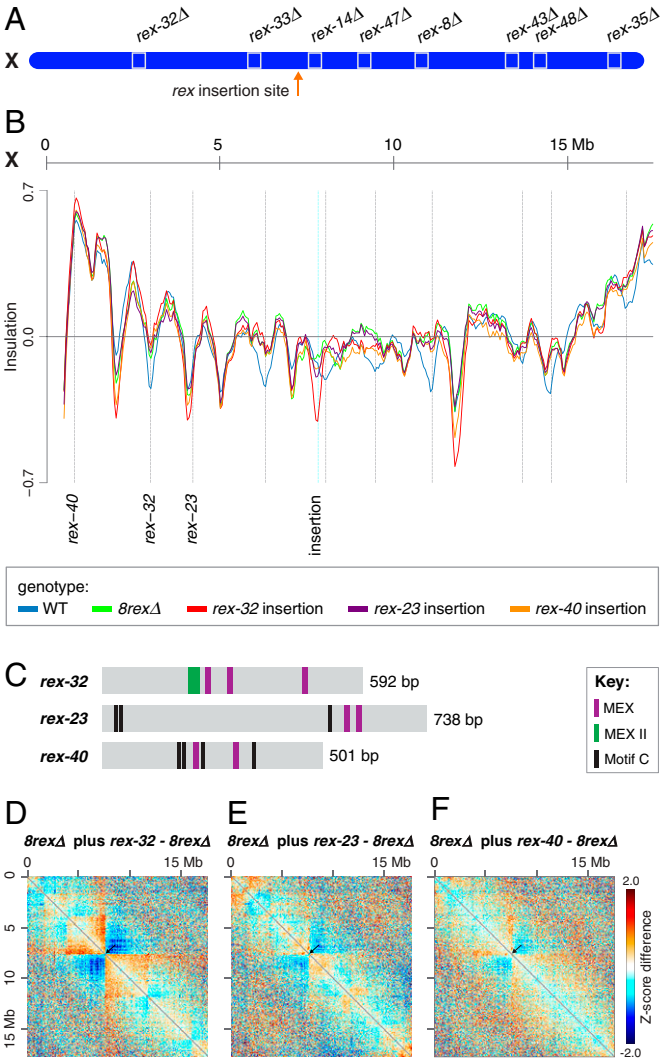

Fig. 6. Contributions of *rex* sites to X-chromosome TAD structure. (*A*) X-chromosome locations of the eight endogenous *rex* sites and their deletions (rectangles) that influence TAD boundary formation. An arrow indicates the site of insertion for *rex-32*, *rex-23*, and *rex-40* on X. (*B*) Plot compares X insulation scores of wild type (blue), *8rexΔ* (green), *8rexΔ* with the *rex-32* insertion (red), *8rexΔ* with the *rex-23* insertion (purple), and *8rexΔ* with the *rex-40* insertion (orange). (*C*) Diagrams of inserted *rex* sites showing motif locations and length. (*D–F*) Z-score subtraction heatmaps (*8rexΔ* plus inserted *rex* minus *8rexΔ*) binned at 50 kb show Hi-C interaction frequencies on X in embryos with an insertion of *rex-32* (*D*), *rex-23* (*E*), or *rex-40* (*F*). The heatmaps demonstrate that high-occupancy *rex* sites (*rex-23* and *rex-40*) that do not form a TAD boundary at their endogenous locations are capable of forming a boundary at a different location. Arrows mark locations of new boundaries. The scale shows the color code for Z-score changes.

with *rex-32* having MEX and MEX II motifs with the strongest matches to the consensus, *rex-23* having less strong MEX motifs, and *rex-40* having the least strong MEX motifs and also Motif C variants comparable to those in *rex-46* (*SI Appendix*, Table S1). These results indicate that both the motif composition of a *rex* site and its location on X contribute to TAD boundary formation.

Discussion

Our work elucidated the strategy by which the *C. elegans* DCC is recruited specifically to X chromosomes. We found that combinations of three different DNA motifs on X recruit the DCC in a synergistic manner to achieve DCC binding in vivo. Our genomics approaches to define DCC binding sites and DNA motifs therein, coupled with validation of motif usage in vivo, revealed two DNA motifs on X that collaborate with the original X-enriched MEX motif to mediate DCC interactions with its recruitment sites (*rex* sites): MEX II, a 26-bp X-enriched motif and Motif C, a 9-bp motif that lacks X enrichment. Individual *rex* sites have diverse combinations of these three different motifs, often clustered together with varying distances between any two motifs, but typically within 50 bp of each other.

Synergy for DCC binding in vivo was demonstrated by quantifying binding in genome-edited strains for which 1) combinations of motifs were added to new locations on X chromosomes lacking DCC binding sites; 2) combinations of the three different X motifs were mutated within endogenous *rex* sites; or 3) motifs were added to endogenous *rex* sites. We found that inserting DNA with MEX and MEX II together into a new location on the X created a DCC binding site equivalent to an endogenous *rex* site, but inserting only MEX or MEX II individually did not. Mutating a single motif at an endogenous *rex* site, MEX, MEX II, or Motif C, dramatically reduced DCC binding in vivo to a level comparable to that of mutating all motifs in the site. Changing the orientation of motifs or altering the spacing between motifs in an endogenous site dramatically reduced the level of DCC binding. Adding a motif to an endogenous site enhanced binding. Hence, synergy achieved through combinatorial clustering of motifs in endogenous *rex* sites triggers DCC assembly specifically on X chromosomes.

To further understand DCC binding to X and to determine the important features and functions of these three motifs, an in vitro assay was developed using embryonic extract. DCC binding was evident not only on *rex* sites with different combinations of the three X motifs but also on X control DNA with insertion of the motifs in different combinations. DCC binding also occurred on templates with only an individual MEX or MEX II motif, as demonstrated using control DNA with insertion of an individual motif or using altered *rex-1* and *rex-39* templates in which only one MEX or MEX II motif remained.

The greater decrease in DCC binding exhibited in vivo than in vitro when eliminating an individual motif in the context of clustered motifs may simply reflect differences in the sensitivity and nature of the assays. However, the need for synergistic interactions in vivo, but not in vitro, could reflect the fact that DCC binding to *rex* sites in vivo would have to compete with nucleosomes (*SI Appendix*, Fig. S4 and data from ref. 35), or general chromatin binding proteins and transcription factors, as shown in prior studies (26, 35), while binding in vitro would not be confounded by such competition.

The ability of the in vitro assay to detect DCC binding to a single motif permitted us to determine key sequence features within motifs. For the 26-bp MEX II motif, which includes three separate regions of conserved sequences, mutating each region individually reduced binding in vitro, indicating that highly conserved elements within MEX II contribute to DCC binding. For the 12-bp MEX motif, mutations in 11 of 12 individual nucleotides reduced DCC binding, demonstrating the importance of individual nucleotides in DCC binding. For experiments conducted in vivo, some of the single mutations in the *rex-1* MEX motif caused a smaller decrease in DCC binding than the same mutations caused for DCC binding in vitro. The template used in vitro included only a MEX motif. The synergy in DCC binding between the mutated MEX motif and the wild-type MEX II motif in *rex-1* likely accounts for the difference.

Analysis of Motif C in vitro revealed the important contribution of flanking sequences to DCC binding. While the presence of the best-scoring Motif C permitted some DCC binding in the context of a *rex-46* template lacking the two other motifs, the identical Motif C inserted into control DNA did not result in DCC binding. Moreover, when all three Motif C variants were inserted into control DNA, DCC binding was not evident. Only when sequences between the Motif C variants were included did DCC binding reach the level of that on the wild-type *rex-46* template. This result demonstrated that DNA sequences surrounding the motifs facilitate DCC binding. The importance of flanking DNA for DCC binding was also evident for motifs at other *rex* sites. A single MEX motif in *rex-1* had greater DCC binding compared to the same MEX motif inserted into control DNA. Furthermore, mutating only the spacer sequence between the MEX and MEX II motifs of *rex-1*, while maintaining the same spacer length as the wild-type spacer, compromised DCC binding in vitro. Both results show that DNA sequences surrounding a motif can modulate DCC binding.

All three X motifs share the core consensus sequence CAGGG. The conservation of this sequence most likely reflects a common mode of interactions between the three DNA motifs and a DNA binding domain for at least one of the dosage compensation proteins. The fact that the unique 5′ end of MEX II is required for optimal DCC binding in vitro likely reflects a different mode of DNA–protein interactions than that for the CAGGG core. These unique interactions could be with an as-yet unidentified DNA binding protein within the DCC or instead with different subunits of the DCC or a different domain of a single DNA binding subunit that interacts with CAGGG sequences. The need for three copies of Motif C to attain maximal DCC binding in vitro may reflect weaker interactions between Motif C and its binding protein than the interactions between MEX or MEX II and relevant binding proteins. More systematic dissection of DCC binding to DNA motifs using purified DCC components will be essential to identify the subunits that bind directly to the three X motifs and the interactions between proteins and DNA motifs that mediate DCC binding and the resultant DCC assembly along X chromosomes.

The occurrence of multiple *rex* sites on X plausibly contributes to synergy in DCC binding through the principle of mass action. A high local DCC concentration along X could facilitate a decrease in the protein–DNA search time required for DCC subunits to find and bind a site. Additionally, interactions between DCC complexes bound to motifs within and between *rex* sites would result in a higher probability of maintaining DCC binding on X and facilitate DCC binding to *rex* sites inserted into new locations on X.

In contrast, DCC binding to autosomes is rare, because the conditions that facilitate synergy in DCC binding on X do not occur on autosomes. The motifs are infrequent, not clustered, and have poor matches to X consensus motifs. Unlike on X, insertion of a high-occupancy *rex* site with multiple motifs on autosomes does not result in DCC binding, because DCC binding sites are not present on autosomes to facilitate DCC binding to

an inserted site through mass action. Even inserting three *rex* sites on an autosome permits only modest DCC binding, and the binding is minimal compared to that at the same sites on X (18).

The synergy in DCC binding to X has parallels with the cooperativity in binding of bacteriophage λ repressor to its operator sites (36). Cooperativity in repressor binding to its multiple sites permits the phage to turn off expression of its essential growth genes, activate expression of its own repressor gene, and thereby remain integrated into its bacterial host genome under favorable bacterial growth conditions. During unfavorable growth conditions, the domain required for cooperative binding is cleaved off, permitting the phage to excise rapidly from its host genome and replicate. Future DCC binding experiments conducted in vitro will reveal the strength of DCC subunit interactions in binding to individual motifs and motif clusters and elucidate the nature of any potential interactions between DCC complexes that enhance binding to facilitate DCC assembly along X chromosomes.

Not only has our study revealed important properties of DCC binding to X chromosomes, it has clarified the role of *rex* sites in creating the three-dimensional structure of X chromosomes. DCC binding at some of the highest-occupancy *rex* sites creates self-interacting domains on X that resemble mammalian TADs (17, 18). However, DCC binding at other equivalently high-occupancy *rex* sites does not. We asked whether the difference in capacity to form a TAD boundary was due to the motif composition of the *rex* site or to the location of the *rex* site on X. The boundary-forming ability of a *rex* site could be masked by its proximity to a chromosome end (*rex-40*) or another TAD boundary (*rex-23*). By inserting these high-occupancy *rex* sites that failed to form TAD boundaries at their endogenous locations into new locations on X, we found that these *rex* sites were capable of establishing TAD boundaries at the new locations. The magnitude of the boundary was directly correlated with the DCC binding capability of the *rex* site. Hence, both the location of a *rex* site and its motif composition dictate whether it can create a TAD boundary. In summary, analysis of dosage compensation in *C. elegans* has revealed general principles by which a large protein complex can be recruited across an entire chromosome to control its structure and gene expression.

Materials and Methods

Genome Editing. Genome editing using Cas9 to create nematode strains with mutant forms of endogenous *rex* sites was performed as described previously (37).

Analysis of DCC Binding In Vivo. The level of DCC binding in vivo along X chromosomes and at both wild-type and mutant *rex* sites was assessed as described previously (18).

Chromosome Structure Analysis. Hi-C analysis to determine chromosome structure was conducted as described previously (18, 23).

For further details, refer to *SI Appendix, SI Materials and Methods*.

Data, Materials, and Software Availability. The accession no. for the ChIP-seq data (38) and Hi-C data (38) reported in this paper is GEO GSE205949.

ACKNOWLEDGMENTS. We are grateful to D. Lapidus for performing Cas9-mediated genome editing to help create strains with mutations in Motif C variants, to C. Preston for nucleosome data, to D. Stalford for masterful figure design, to T. Cline and the B.J.M. laboratory members for valuable discussions, and to the QB3 Genomics Facility (RRID:SCR_022170) for DNA sequencing. This work was supported in part by NIH Grant R35 GM131845 (to B.J.M.). B.J.M. is an investigator of the Howard Hughes Medical Institute.

Author affiliations: [a]HHMI, University of California, Berkeley, CA 94720; and [b]Department of Molecular and Cell Biology, University of California, Berkeley, CA 94720

1. J. J. Siegel, A. Amon, New insights into the troubles of aneuploidy. *Annu. Rev. Cell Dev. Biol.* **28**, 189–214 (2012).
2. U. Ben-David, A. Amon, Context is everything: Aneuploidy in cancer. *Nat. Rev. Genet.* **21**, 44–62 (2020).
3. A. Loda, S. Collombet, E. Heard, Gene regulation in time and space during X-chromosome inactivation. *Nat. Rev. Mol. Cell Biol.* **23**, 231–249 (2022).
4. B. J. Meyer, Mechanisms of sex determination and X-chromosome dosage compensation. *Genetics* **220**, iyab197 (2022).
5. B. J. Meyer, The X chromosome in *C. elegans* sex determination and dosage compensation. *Curr. Opin. Genet. Dev.* **74**, 101912 (2022).
6. M. Samata, A. Akhtar, Dosage compensation of the X chromosome: A complex epigenetic assignment involving chromatin regulators and long noncoding RNAs. *Annu. Rev. Biochem.* **87**, 323–350 (2018).
7. L. E. Rieder, W. T. Jordan, 3rd, E. N. Larschan, Targeting of the dosage-compensated male X-chromosome during early *Drosophila* development. *Cell Rep.* **29**, 4268–4275.e2 (2019).
8. H. Yin, C. Wei, J. T. Lee, Revisiting the consequences of deleting the X inactivation center. *Proc. Natl. Acad. Sci. U.S.A.* **118**, e2102683118 (2021).
9. W. Jordan, 3rd, L. E. Rieder, E. Larschan, Diverse genome topologies characterize dosage compensation across species. *Trends Genet.* **35**, 308–315 (2019).
10. W. S. Kruesi, L. J. Core, C. T. Waters, J. T. Lis, B. J. Meyer, Condensin controls recruitment of RNA polymerase II to achieve nematode X-chromosome dosage compensation. *eLife* **2**, e00808 (2013).
11. W. Jordan, 3rd, E. Larschan, The zinc finger protein CLAMP promotes long-range chromatin interactions that mediate dosage compensation of the *Drosophila* male X-chromosome. *Epigenetics Chromatin* **14**, 29 (2021).
12. P. T. Chuang, D. G. Albertson, B. J. Meyer, DPY-27:a chromosome condensation protein homolog that regulates *C. elegans* dosage compensation through association with the X chromosome. *Cell* **79**, 459–474 (1994).
13. J. D. Lieb, M. R. Albrecht, P. T. Chuang, B. J. Meyer, MIX-1: An essential component of the *C. elegans* mitotic machinery executes X chromosome dosage compensation. *Cell* **92**, 265–277 (1998).
14. G. Csankovszki *et al.*, Three distinct condensin complexes control *C. elegans* chromosome dynamics. *Curr. Biol.* **19**, 9–19 (2009).
15. D. G. Mets, B. J. Meyer, Condensins regulate meiotic DNA break distribution, thus crossover frequency, by controlling chromosome structure. *Cell* **139**, 73–86 (2009).
16. S. Yatskevich, J. Rhodes, K. Nasmyth, Organization of chromosomal DNA by SMC complexes. *Annu. Rev. Genet.* **53**, 445–482 (2019).
17. E. Crane *et al.*, Condensin-driven remodelling of X chromosome topology during dosage compensation. *Nature* **523**, 240–244 (2015).
18. E. C. Anderson *et al.*, X chromosome domain architecture regulates *Caenorhabditis elegans* lifespan but not dosage compensation. *Dev. Cell* **51**, 192–207.e6 (2019).
19. H. E. Dawes *et al.*, Dosage compensation proteins targeted to X chromosomes by a determinant of hermaphrodite fate. *Science* **284**, 1800–1804 (1999).
20. T. L. Davis, B. J. Meyer, SDC-3 coordinates the assembly of a dosage compensation complex on the nematode X chromosome. *Development* **124**, 1019–1031 (1997).
21. P. T. Chuang, J. D. Lieb, B. J. Meyer, Sex-specific assembly of a dosage compensation complex on the nematode X chromosome. *Science* **274**, 1736–1739 (1996).
22. R. R. Pferdehirt, W. S. Kruesi, B. J. Meyer, An MLL/COMPASS subunit functions in the *C. elegans* dosage compensation complex to target X chromosomes for transcriptional regulation of gene expression. *Genes Dev.* **25**, 499–515 (2011).
23. K. Brejc *et al.*, Dynamic control of X chromosome conformation and repression by a histone H4K20 demethylase. *Cell* **171**, 85–102.e23 (2017).
24. P. McDonel, J. Jans, B. K. Peterson, B. J. Meyer, Clustered DNA motifs mark X chromosomes for repression by a dosage compensation complex. *Nature* **444**, 614–618 (2006).
25. J. Jans *et al.*, A condensin-like dosage compensation complex acts at a distance to control expression throughout the genome. *Genes Dev.* **23**, 602–618 (2009).
26. S. E. Albritton, A. L. Kranz, L. H. Winterkorn, L. A. Street, S. Ercan, Cooperation between a hierarchical set of recruitment sites targets the X chromosome for dosage compensation. *eLife* **6**, e23645 (2017).
27. G. Csankovszki, P. McDonel, B. J. Meyer, Recruitment and spreading of the *C. elegans* dosage compensation complex along X chromosomes. *Science* **303**, 1182–1185 (2004).
28. R. R. Pferdehirt, B. J. Meyer, SUMOylation is essential for sex-specific assembly of the *C. elegans* dosage compensation complex onto the X chromosomes. *Proc. Natl. Acad. Sci. U.S.A.* **110**, E3810–E3819 (2013).
29. B. S. Wheeler *et al.*, Chromosome-wide mechanisms to decouple gene expression from gene dose during sex-chromosome evolution. *eLife* **5**, e17365 (2016).
30. G. Z. Hertz, G. D. Stormo, Identifying DNA and protein patterns with statistically significant alignments of multiple sequences. *Bioinformatics* **15**, 563–577 (1999).
31. T. L. Bailey, C. Elkan, Fitting a mixture model by expectation maximization to discover motifs in biopolymers. *Proc. Int. Conf. Intell. Syst. Mol. Biol.* **2**, 28–36 (1994).
32. J. R. Dixon *et al.*, Topological domains in mammalian genomes identified by analysis of chromatin interactions. *Nature* **485**, 376–380 (2012).
33. E. P. Nora *et al.*, Spatial partitioning of the regulatory landscape of the X-inactivation centre. *Nature* **485**, 381–385 (2012).
34. J. A. Beagan, J. E. Phillips-Cremins, On the existence and functionality of topologically associating domains. *Nat. Genet.* **52**, 8–16 (2020).
35. C. G. Preston, "Nucleosome occupancy and modification in *C. elegans* dosage compensation," PhD thesis in Molecular and Cell Biology, University of California, Berkeley, CA (2014).
36. M. Ptashne, *A Genetic Switch: Phage Lambda and Higher Organisms* (Cell Press: Blackwell Scientific Publications, Cambridge, MA, ed. 2, 1992), pp. 1–33.
37. B. Farboud, A. F. Severson, B. J. Meyer, Strategies for efficient genome editing using CRISPR-Cas9. *Genetics* **211**, 431–457 (2019).
38. N. Fuda *et al.*, Data from "Combinatorial clustering of distinct DNA motifs directs synergistic binding of *C. elegans* dosage compensation complex to X chromosomes." https://www.ncbi.nlm.nih.gov/geo/query/acc.cgi?acc=GSE205949. Deposited 10 June 2022.